JCI The Journal of Clinical Investigation

Measles virus blind to its epithelial cell receptor remains virulent in rhesus monkeys but cannot cross the airway epithelium and is not shed

Vincent H.J. Leonard, … , Michael B. McChesney, Roberto Cattaneo

J Clin Invest. 2008;118(7):2448-2458. https://doi.org/10.1172/JCI35454.

Research Article

The current model of measles virus (MV) pathogenesis implies that apical infection of airway epithelial cells precedes systemic spread. An alternative model suggests that primarily infected lymphatic cells carry MV to the basolateral surface of epithelial cells, supporting MV shedding into the airway lumen and contagion. This model predicts that a mutant MV, unable to enter cells through the unidentified epithelial cell receptor (EpR), would remain virulent but not be shed. To test this model, we identified residues of the MV attachment protein sustaining EpR-mediated cell fusion. These nonpolar or uncharged polar residues defined an area located near the binding site of the signaling lymphocytic activation molecule (SLAM), the receptor for MV on lymphatic cells. We then generated an EpR-blind virus maintaining SLAM-dependent cell entry and inoculated rhesus monkeys intranasally. Hosts infected with the selectively EpR-blind MV developed rash and anorexia while averaging slightly lower viremia than hosts infected with wild-type MV but did not shed virus in the airways. The mechanism restricting shedding was characterized using primary well-differentiated human airway epithelial cells. Wild-type MV infected columnar epithelial cells bearing tight junctions only when applied basolaterally, while the EpR-blind virus did not infect these cells. Thus, EpR is probably a basolateral protein, and infection of the airway epithelium is not essential for systemic spread and virulence of MV.

 Related Commentary, page 2386

Measles virus blind to its epithelial cell receptor remains virulent in rhesus monkeys but cannot cross the airway epithelium and is not shed

Vincent H.J. Leonard,[1] Patrick L. Sinn,[2] Gregory Hodge,[3] Tanner Miest,[1] Patricia Devaux,[1] Numan Oezguen,[4] Werner Braun,[4] Paul B. McCray Jr.,[2] Michael B. McChesney,[3] and Roberto Cattaneo[1]

[1]Department of Molecular Medicine, Mayo Clinic, Rochester, Minnesota, USA. [2]Department of Pediatrics, University of Iowa Carver College of Medicine, Iowa City, Iowa, USA. [3]California National Primate Research Center and Department of Pathology and Laboratory Medicine, UC Davis School of Medicine, Davis, California, USA. [4]Sealy Center for Structural Biology, University of Texas Medical Branch, Galveston, Texas, USA.

The current model of measles virus (MV) pathogenesis implies that apical infection of airway epithelial cells precedes systemic spread. An alternative model suggests that primarily infected lymphatic cells carry MV to the basolateral surface of epithelial cells, supporting MV shedding into the airway lumen and contagion. This model predicts that a mutant MV, unable to enter cells through the unidentified epithelial cell receptor (EpR), would remain virulent but not be shed. To test this model, we identified residues of the MV attachment protein sustaining EpR-mediated cell fusion. These nonpolar or uncharged polar residues defined an area located near the binding site of the signaling lymphocytic activation molecule (SLAM), the receptor for MV on lymphatic cells. We then generated an EpR-blind virus maintaining SLAM-dependent cell entry and inoculated rhesus monkeys intranasally. Hosts infected with the selectively EpR-blind MV developed rash and anorexia while averaging slightly lower viremia than hosts infected with wild-type MV but did not shed virus in the airways. The mechanism restricting shedding was characterized using primary well-differentiated human airway epithelial cells. Wild-type MV infected columnar epithelial cells bearing tight junctions only when applied basolaterally, while the EpR-blind virus did not infect these cells. Thus, EpR is probably a basolateral protein, and infection of the airway epithelium is not essential for systemic spread and virulence of MV.

Introduction

Measles virus (MV) is one of the most contagious human pathogens (1). It is transmitted by aerosols, infecting a new host via the upper respiratory tract. It is currently thought that MV, a member of the *Morbillivirus* genus of the Paramyxoviridae family, infects the upper respiratory epithelium from the luminal side before spreading in lymphatic cells (2, 3). It is undisputed that eventually, MV infection can spread to many organs including the respiratory tract (4–6). However, no direct evidence exists for primary MV replication in respiratory epithelial cells, whereas rapid and massive spread of morbillivirus infection through lymphatic cells expressing the signaling lymphocytic activation molecule (SLAM; CD150) (7) was recently documented (8).

Thus, a new model postulating that systemic spread of wild-type MV depends only on infection of SLAM-expressing lymphatic cells, without initial virus amplification in respiratory epithelial cells, was proposed (8–10). This model implies that MV does not cross the respiratory epithelium immediately after infection, but only when it leaves the host. In this alternative model, crossing occurs only from the basolateral to the apical side, suggesting that the elusive epithelial receptor (EpR) is located basolaterally. Consistent with this prediction, studies based on transformed cell lines reported that formation of a polarized monolayer interfered with apical infection (11, 12). Moreover, studies based on primary well-differentiated human airway epithelium showed that a vaccine strain MV preferentially infects these epithelia from the basolateral surface (13), but the question of the polarity of infection of wild-type MV was not asked in this system.

To test whether MV spread and virulence depend only on infection of SLAM-expressing lymphatic cells, we sought to generate a virus that cannot recognize EpR but maintains SLAM-dependent entry. MV contacts its receptors through the attachment protein hemagglutinin. The H protein homodimer supports membrane fusion and viral entry together with the trimeric fusion (F) protein (14, 15). We have previously shown that receptor-specific cell-to-cell fusion assays can be used to identify H protein amino acids involved in fusion support, and that selectively receptor-blind MV can be generated (16). This work was based on cell lines expressing either SLAM, the lymphatic cell receptor for all MV strains, or the membrane cofactor protein (MCP; CD46), a ubiquitous protein that is recognized only by vaccine strains (17, 18).

We now extend the virus-receptor interaction characterization and de-targeting principle to the unidentified EpR. Toward this, we first identified 3 human epithelial cell lines susceptible to wild-type MV infection, thus expressing the putative EpR. Second, we used these cell lines, in combination with a structural model of

Nonstandard abbreviations used: CDV, canine distemper virus; EpR, epithelial receptor; F, fusion (protein); H, hemagglutinin (protein); MV, measles virus; SLAM, signaling lymphocytic activation molecule; $TCID_{50}$, tissue culture infectious dose 50%.

Conflict of interest: The authors have declared that no conflict of interest exists.

Citation for this article: *J. Clin. Invest.* **118**:2448–2458 (2008). doi:10.1172/JCI35454.

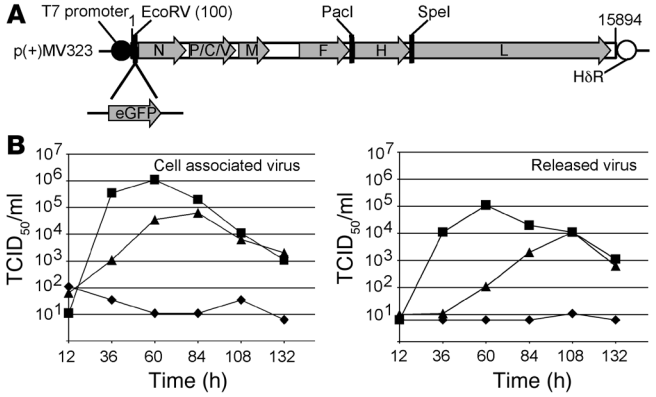

Figure 1
Wild-type MV infects human epithelial cells independently of SLAM. (**A**) Map of the p(+)MV323 plasmid coding for the WT genome and location of the inserted GFP gene. The coding regions of MV genes are represented by arrow-shaped gray boxes. The T7 promoter hepatitis delta virus ribozyme (HδR) and selected unique restriction sites are indicated. The EGFP transcriptional unit was inserted at an EcoRV restriction site downstream of the *N* gene transcription start. (**B**) Viral growth kinetics of cell-associated (left) or released (right) WT_{green} following infection of H358 (triangles), Vero/hSLAM (squares), or Vero (diamonds) cells. Viral titers (mean of 2 measurements) are indicated as $TCID_{50}$/ml.

H protein and mutational analysis, to identify and locate residues in H protein sustaining EpR-dependent fusion. Third, we generated an EpR-blind virus. This MV remained virulent in rhesus monkeys but was not shed.

Results

MV infects human epithelial cells independently of SLAM. To facilitate analysis of the permissivity of human epithelial cell lines to wild-type MV infection, the wild-type molecular clone MVwtIC323 (herein referred to as WT) was engineered to express GFP from an additional transcription unit (Figure 1A). Titers of WT_{green} were equivalent to those of WT, and the 2 strains exhibited equal kinetics.

To identify permissive epithelial cells, 7 transformed cell lines of different origin were chosen: H358 and H441 are bronchoalveolar carcinoma and papillary adenocarcinoma cells, respectively, whereas H23 and H522 cells derive from adenocarcinoma. In addition, 3 carcinoma cell lines derived from the human urinary transitional epithelium were selected: SCaBER, T24, and HT-1376. WT_{green} infected H358 and H441 lung cells and HT-1376 bladder cells but not the other epithelial cell lines tested (Table 1). As expected, this wild-type virus infected control cell lines expressing SLAM (B95a and Vero/hSLAM cells) but not control cell lines expressing only CD46 (Vero and HeLa cells). SLAM, the only known receptor for wild-type MV, was not detected by flow cytometry on the surface of HT-1376, H441, and H358 cells (data not shown). The vaccine lineage $MVvacNSe_{green}$ (19) infected every cell type tested, probably through the ubiquitous protein CD46. Thus, we identified 3 cell lines from MV target organs expressing an unidentified receptor, EpR, allowing wild-type MV entry.

To compare growth of the wild-type virus on EpR- and SLAM-expressing cells, the infection of H358, Vero/hSLAM, and Vero cells by WT_{green} was monitored over 6 days (Figure 1B). In H358 cells (triangles), the virus replicated efficiently, reaching a titer of nearly 10^5 tissue culture infectious dose 50% ($TCID_{50}$)/ml for cell-associated virus and 10^4 $TCID_{50}$/ml for released virus. These titers were about 10-fold lower than those in Vero/hSLAM cells (squares). The peak of viral production was delayed in H358 compared with Vero/hSLAM cells. As expected, viral production in Vero cells (diamonds) was at background levels.

To assess whether other wild-type strains infect H358 cells, we used 3 clinical isolates (MVwtD4, MVwtD8, and MVwtH1) known to enter cells via SLAM but not CD46 (20). These viruses produced syncytia within 48 hours (Supplemental Figure 1; supplemental material available online with this article; doi:10.1172/JCI35454DS1; similar observations were recently reported; ref. 21). Taken together, these data confirm the presence of an unidentified receptor, EpR, for wild-type MV on the surface of certain human lung and bladder epithelial cells, sustaining virion-to-cell and cell-to-cell fusion.

Residues in H protein β-sheets 4 and 5 sustain EpR-dependent fusion. To identify residues in H protein required for EpR-dependent fusion support, we used an iterative mutagenesis protocol and assays measuring EpR- or SLAM-dependent fusion. Based on analyses of the H protein residues or epitopes available for interaction (16, 22–24), we focused mutagenesis on amino acids 382–617. We hypothesized that the EpR interaction is conserved within viruses of the *Morbillivirus* genus, as is the case for SLAM binding, and therefore mutated all the H protein amino acids conserved among the 3 morbilliviruses: MV, rinderpest virus (RV), and canine distemper virus (CDV) (Figure 2A). Alanine and serine were used to substitute polar and apolar residues, respectively. Conserved cysteine and tryptophan residues were not mutated to preserve protein structure and the hydrophobic core. The fusogenic activity of 48 mutant proteins was scored in 2 fusion assays based on complementation with the F protein, one performed in EpR-expressing H358 cells and the other in SLAM-expressing Vero/hSLAM cells (Figure 2B).

Four residues with EpR-selective fusion support function (I456, L464, P497, and Y543) were identified during the first round of mutagenesis and receptor-dependent functional screening. These residues were located on a model of the wild-type H protein ectodomain (residues 145–617) developed as previously described for a vaccine strain H protein (16). This model, which predicted correctly the global folding of the MV H protein, was used to plan a second round of mutagenesis. All of the amino acids that were

Table 1
MV permissivity of human or primate cells

Cell line	Origin	Permissivity	
		WT_{green}	$MVvacNSe_{green}$
H358	Human lung	+	+
H441	Human lung	+	+
H23	Human lung	–	+
H522	Human lung	–	+
SCaBER	Human urinary bladder	–	+
T24	Human urinary bladder	–	+
HT-1376	Human urinary bladder	+	+
B95a	Marmoset B lymphocyte	+	+
Vero/hSLAM	AGM kidney	+	+
Vero	AGM kidney	–	+
HeLa	Human cervix	–	+

AGM, African green monkey; +, infectible; –, noninfectible.

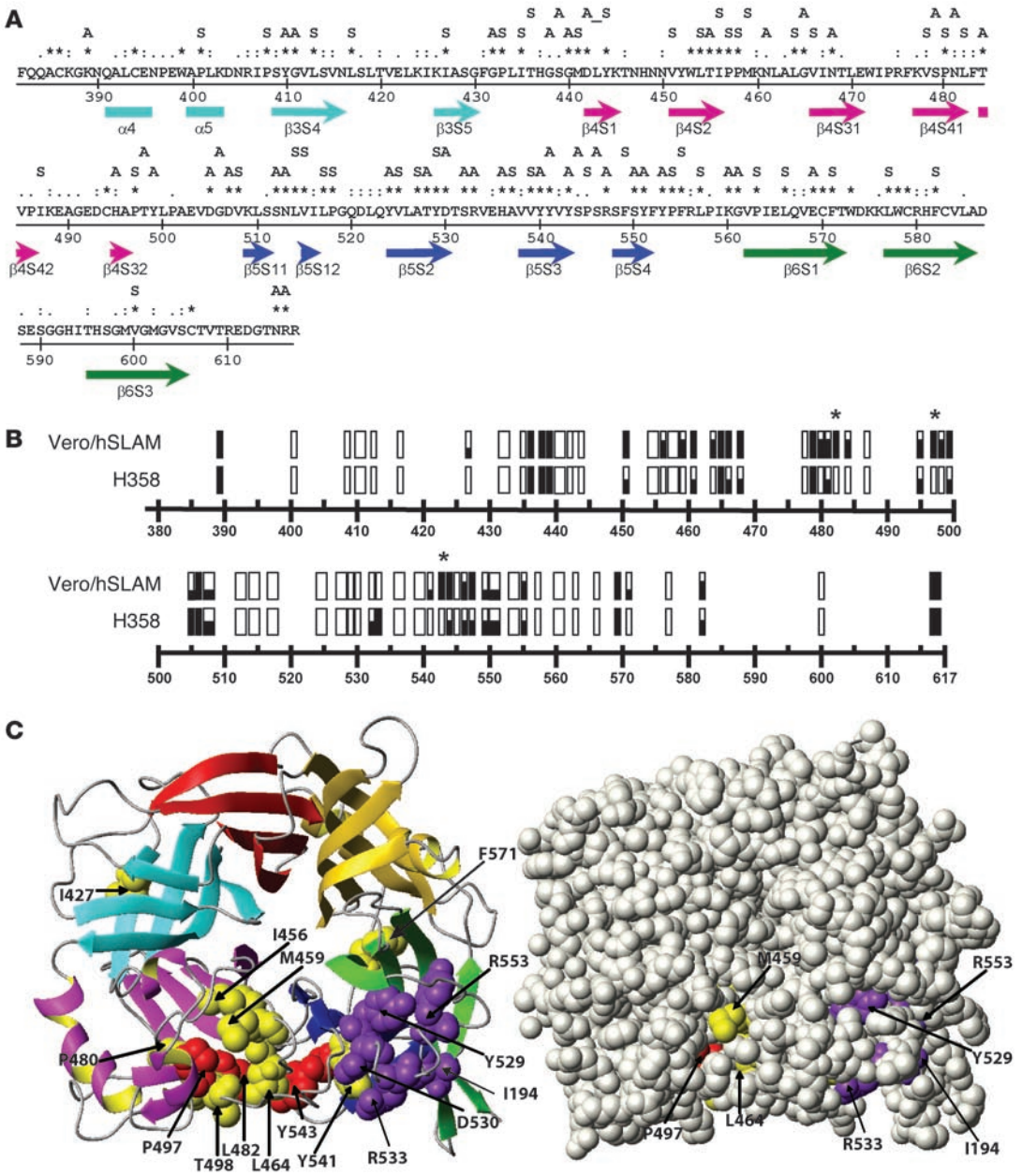

Figure 2

H protein residues relevant for EpR-dependent fusion. (**A**) Amino acid sequence 382–617 of the wild-type MV H protein. Homology of MV to CDV and rinderpest virus (RV) H proteins (NCBI protein sequence database accession numbers NP_056923, AAD18008, and AAD25093) is indicated as follows: asterisks (*), identical residues; colons (:), conserved residues; periods (.), semiconserved residues. The letters above the alignment denote mutants produced as single (individual letter) or double substitutions (contiguous residues; only the double mutant 442–444 is not contiguous) to alanine (A, polar residues) or serine (S, nonpolar residues). The H protein secondary structure is shown below the MV H sequence, with arrows indicating β-strands and boxes indicating α-helixes. Cyan, pink, blue, and green indicate the predicted propeller sheets 3–6, respectively. (**B**) Fusion efficiency of the H protein mutants in Vero/hSLAM or H358 cells. Each mutant is represented as a rectangle located at the appropriate position. Filled rectangles indicate full fusion activity; white rectangles, no fusion activity; partially filled rectangles, intermediate fusion levels. Mutants with unaltered SLAM-mediated fusion and no EpR-mediated fusion are indicated by asterisks. (**C**) Top view of the H protein crystal structure (25) in a ribbon plot (left) and space-filling (right) representation. The structure is color coded as in **A**; β-sheets 1 and 2 are indicated in yellow and red, respectively. Red: residues whose mutation abolished EpR-dependent fusion while completely retaining SLAM-dependent fusion; yellow: residues whose mutation abolished EpR-dependent fusion while strongly or moderately impairing SLAM-dependent fusion function; purple: residues important for SLAM-induced fusion.

predicted to be located within 10 Å of I456, L464, P497, or Y543 and that were solvent exposed were mutated. The results of these 2 rounds of mutagenesis are shown on the recently published H protein crystal structure (25, 26). This structure is visualized in Figure 2C, in a ribbon plot representation (left) and in a space-filling representation (right). Both panels show the H protein structure from the top, illustrating a super-barrel in which 6 β-sheets are arranged cyclically around a central axis.

Of the 69 mutants analyzed, 9 maintained full fusion support in both cell lines (Figure 2B, filled rectangles), and 30 lost fusion capacity in both cell lines (Figure 2B, open rectangles). Twelve mutants had no fusion support capacity in H358 epithelial cells but maintained at least partial fusion support in Vero/hSLAM cells (Figure 2B). Three of these mutants maintained low fusion support in Vero/hSLAM cells (I427S, Y541A, F571S), 6 retained most fusion support (I456S, M459S, L464S, P480S, T484A, T498A), and 3 retained complete SLAM-dependent fusion support (L482S, P497S, Y543A; asterisks in Figure 2B).

These last 3 residues are shown in red on the crystal structure; the 9 residues whose mutation also partially impaired SLAM-dependent fusion are in yellow (Figure 2C). Eight of the 9 yellow residues are clustered in one region of the protein, centered around the 3 red residues and located in β-sheets 4 and 5 (Figure 2C, left panel, pink and blue β-sheets, respectively; see also space-filling representation in the right panel). One residue essential for SLAM binding (isoleucine 194 [I194]) (27) and 4 essential for SLAM-dependent fusion — Y529, D530, R533, and Y553 (16) (purple) — are located on β-sheet 5.

Generation of selectively EpR-blind MV. Toward assessing the role of the EpR in virulence, we sought to generate selectively EpR-blind MV. Among the H protein mutants characterized above, we selected those 3 retaining 100% fusion activity in Vero/hSLAM and without fusion activity in H358 cells (L482S, P497S, and Y543A). These residues have an uncharged polar (Y543) or nonpolar (L482 and P497) side chains. After confirming expression and stability of the corresponding proteins in both cell lines, the mutations were transferred into the WT_{green} backbone to generate WT_{green}-H_{482}; WT_{green}-H_{497}; WT_{green}-H_{543}; and the double mutant with the mutations P497S/Y543A, WT_{green}-H_{DOUBLE}.

As a control, a selectively SLAM-blind wild-type MV was generated. Toward this, the functionality of 4 mutations in the H protein of the vaccine strain known to abrogate SLAM-dependent fusion (Y529A, D530A, R533A, and Y553A) was tested in H358 cells after recloning in the wild-type H protein background. The mutations Y529A, D530A, and Y553A abrogated SLAM-dependent fusion but also partially inhibited EpR-dependent fusion. The mutation R533A preserved fusion capacity in H358 cells and was therefore selected to generate WT_{green}-$H_{SLAMblind}$.

The receptor specificity of the recombinant MV was analyzed on SLAM- or EpR-expressing cell lines (Figure 3). WT_{green}-H_{543} completely lost competence to infect the 3 epithelial cell lines, H358, HT-1376, and H441. WT_{green}-H_{497} and WT_{green}-H_{482} infected these epithelial cells, but with much lower efficiency and greatly reduced fusion capacity compared with WT_{green}. On the other hand, all 3 viruses efficiently infected Vero/hSLAM cells. These results show that WT_{green}-H_{543} is EpR blind and WT_{green}-H_{482} and WT_{green}-H_{497} are EpR-entry impaired. The double mutant WT_{green}-H_{DOUBLE} did not infect any of the epithelial cell lines, but it had somewhat reduced fusion efficiency in Vero/hSLAM cells. WT_{green}-$H_{SLAMblind}$ was unable to infect Vero/hSLAM cells but efficiently infected the 3 epithelial cell lines. None of the recombinant viruses infected Vero cells, confirming a lack of interaction with CD46. Thus, we have generated selectively EpR- and selectively SLAM-blind mutant MVs.

A selectively EpR-blind MV remains virulent in monkeys. To assess the role of the EpR in virulence, we used the rhesus monkey (*Macaca mulatta*), a primate species that develops the clinical signs of measles when infected with wild-type MV. To minimize the probability of selecting revertants during viral replication in the host, a virus with 2 mutations in EpR recognition was sought. To avoid possible loss of virulence due to reporter protein expression (28), a variant of WT_{green}-H_{DOUBLE} not expressing GFP was generated and named WT-H_{DOUBLE}. When WT-H_{DOUBLE} was grown on Vero/hSLAM cells, it reached titers equivalent to those of WT, but with slightly delayed kinetics (Figure 4A). We also verified that WT_{green}-H_{DOUBLE} lost the capacity to infect a lung epithelium cell line of *M. mulatta* (catalog no. CCL-208; ATCC), while WT_{green} did not (data not shown).

Six animals were inoculated intranasally with WT-H_{DOUBLE} using the same conditions we previously used for WT infections (29). Since MV infectivity is strongly cell associated, in monkey and human studies the number of cells per million PBMCs was used as a measure of viremia. WT-H_{DOUBLE} was detected in the PBMCs of all 6 hosts at day 7 after inoculation, the peak of viremia in monkeys infected with WT (29), at titers about 10-fold lower than those of WT (Figure 4B). Similarly, titers 5- to 10-fold lower than for the WT were detected 14 days after inoculation, with 4 animals having cleared infection. Slightly delayed WT-H_{DOUBLE} replication (Figure 4A) may account for slightly lower levels of viremia.

Development of clinical signs was followed over 28 days (Table 2). WT-H_{DOUBLE}–infected macaques developed measles signs comparable to those of the animals infected with WT (29), including skin rash and anorexia. We note that the rash is due to the accumulation of infected and noninfected inflammatory immune cells rather than to infection of epithelial cells (10). The humoral immune response, as reflected in titers and kinetics of neutralizing antibodies, was similar in animals inoculated with WT-H_{DOUBLE} and WT (Figure 4C). Thus, the EpR-blind MV remained virulent in macaques.

No infectivity is shed in the airways of monkeys infected with a selectively EpR-blind MV. Since in our previous study of WT infection, no airway samples were collected (29), we compared this aspect of the WT-H_{DOUBLE} studies with the results of de Swart et al. (10). These authors infected 3 rhesus and 3 cynomolgus monkeys with the same wild-type MV strain IC323 (WT) and reported average peak viremia of about 2×10^3 infectious units per million PBMCs. This is equivalent to the average peak titer documented in our previous study (Figure 4B) (29). De Swart et al. collected throat swabs, nose swabs, and bronchoalveolar lavages and detected WT in all these samples; the peak viral load detected in bronchoalveolar lavage cells ranged from 10^3 to 10^4 infected cells per million (10). It is remarkable that 1:100 to 1:1,000 ratios of infected to noninfected cells were documented in both PBMCs and bronchoalveolar lavages (10).

We collected tracheal aspirates from all monkeys infected with WT-H_{DOUBLE} at 7, 14, 21, and 28 days following inoculation, but we could not isolate virus from any of these samples (Figure 4B; the detection limit was 1 infectious unit in 10^5 to 10^6 cells cocultured with Raji cells). Since we documented peak viremia ranging from 1.5×10^2 to 1.0×10^3 infected cells per million PBMCs in individual

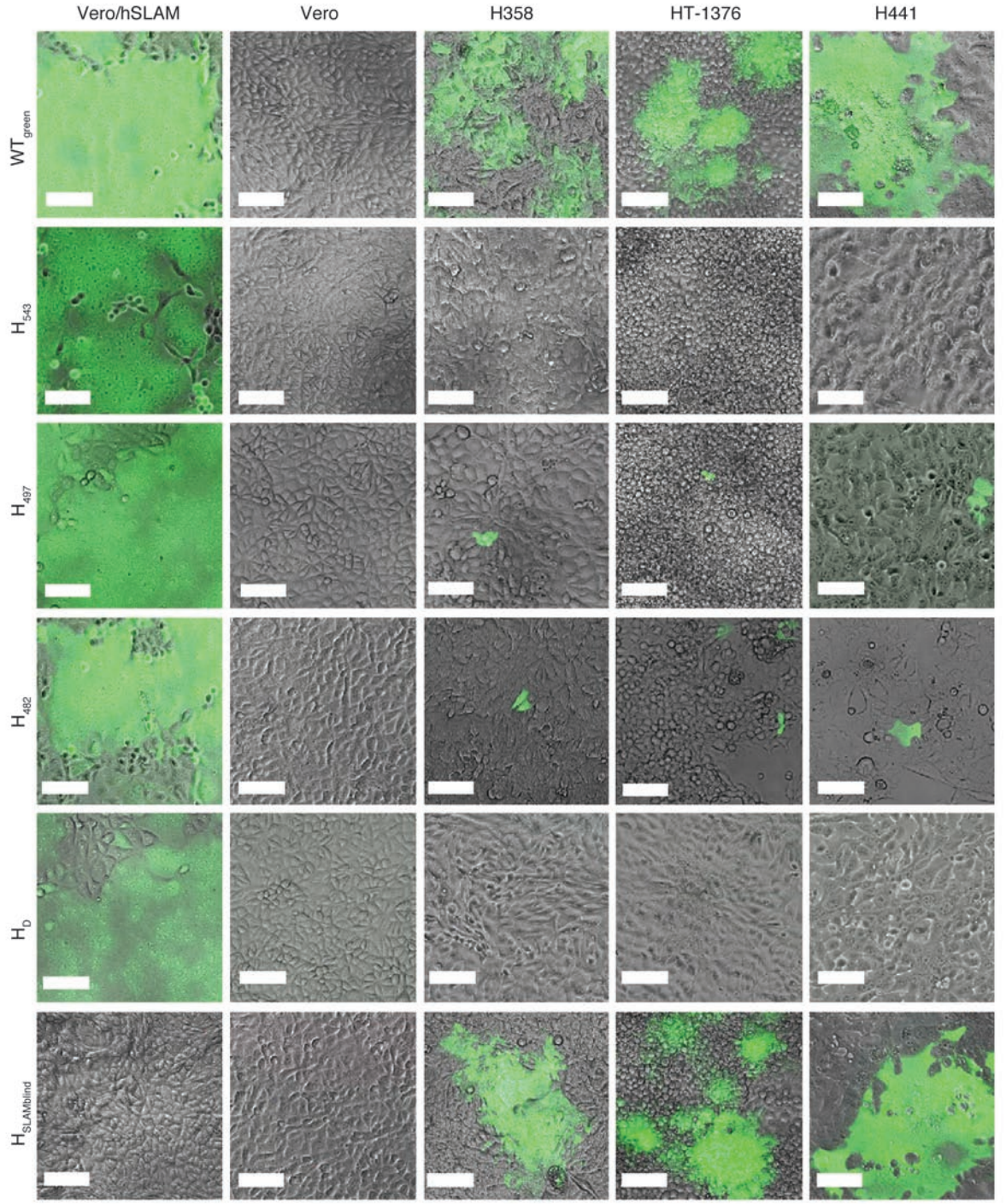

Figure 3
Infectivity of EpR- and SLAM-blind recombinant viruses. WT_{green} and the mutant viruses WT_{green}-H_{543} (H_{543}), WT_{green}-H_{497} (H_{497}), WT_{green}-H_{482} (H_{482}), WT_{green}-H_{DOUBLE} (H_D), and WT_{green}-$H_{SLAMblind}$ ($H_{SLAMblind}$) were used to infect Vero/hSLAM cells, Vero cells, or the 3 epithelial cell lines H358, HT-1376, and H441. The phase-contrast pictures of the cells were overlaid with fluorescence microscopic images. Scale bars: 100 μm.

monkeys infected with WT-H_{DOUBLE} and no virus in their tracheal aspirates, and considering the WT shedding data published by de Swart et al., we estimate that WT-$_{DOUBLE}$ was shed on average at least 100-fold less efficiently than WT.

Wild-type MV uses EpR to enter human airway epithelium basolaterally. To characterize the polarity of MV entry into respiratory epithelium, we used primary cultures of well-differentiated human airway epithelial cells. This reconstituted epithelial sheet, cultured at an air-liquid interface, closely resembles the human airway. The primary cells develop tight junctions and a well-differentiated morphology consisting of a pseudostratified, ciliated columnar epithelium with goblet and basal cells (30). We have previously shown

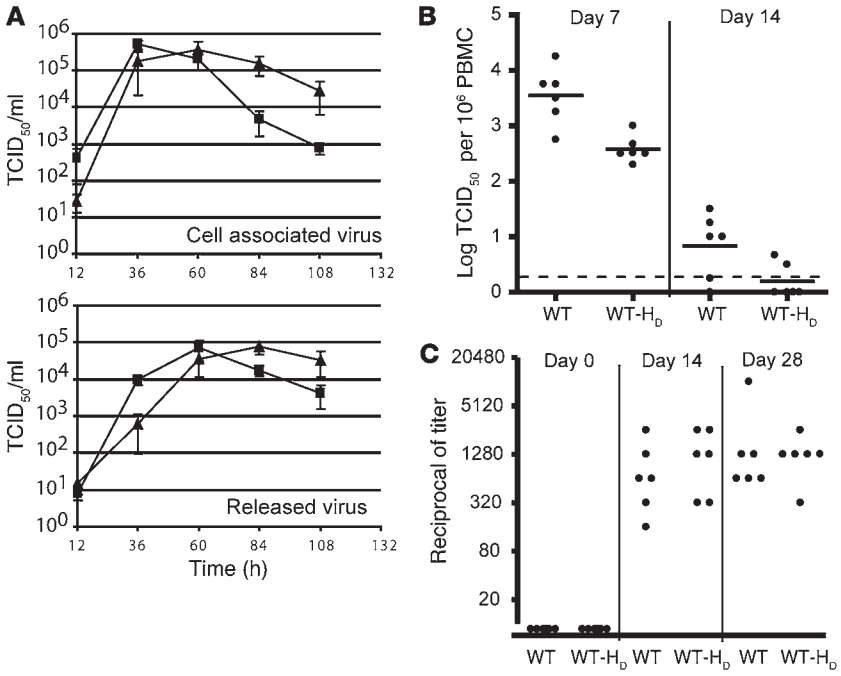

Figure 4
Growth kinetics of an EpR-blind MV and analysis of its virulence in rhesus macaques. (**A**) Kinetics of the production of cell-associated (top) or released (bottom) WT (squares) and WT-H_{DOUBLE} (triangles) in Vero/hSLAM cells. Viral titers are indicated as $TCID_{50}$/ml. Error bars indicate mean ± SD; $n = 3$. (**B**) Titration of viremia in blood samples taken on days 7 or 14 after inoculation of 6 animals infected with $10^{4.5}$ $TCID_{50}$ WT-H_{DOUBLE} (WT-H_D). Each dot represents 1 animal; the mean for the group is indicated by a horizontal bar. The dashed line represents the limit of detection. Data for WT infections are from ref. 29. (**C**) Neutralizing antibody response. Sera obtained at 0, 14, and 28 days after inoculation were assayed for MV neutralization, and results are presented as reciprocals of the titer. Each dot represents an animal. Data for infections with WT are from ref. 29.

that $MVvacNSe_{green}$, a CD46-binding vaccine strain, preferentially infects these epithelial sheets from the basolateral side (13).

WT_{green}, WT_{green}-$H_{SLAMblind}$, $MVvacNSe_{green}$, and the 2 EpR-blind viruses, WT_{green}-H_{543} and WT_{green}-H_{DOUBLE}, were applied at an MOI of 0.1 to either the apical or basolateral surface of epithelial sheets. Infection was quantified by measurement of EGFP fluorescence. As shown in Figure 5A, infection with WT_{green} was detected only upon virus application to the basolateral surface. Infection efficiency was 100- to 300-fold lower than in SLAM-expressing cells, as 0.3–1 infectious centers per 1,000 cells were detected. WT_{green}-$H_{SLAMblind}$ was as efficient as WT_{green} in basolateral infection. In contrast, application of WT_{green}-H_{543} and WT_{green}-H_{DOUBLE} at either the apical or basolateral cell surface resulted in no detectable infection, demonstrating a specific requirement for EpR.

Sequential observation of epithelial sheets infected with WT_{green} using confocal microscopy revealed infectious centers that increased in size over time, but cells remained well defined, and syncytia did not form (Figure 5B). Moreover, these observations revealed cell-type selectivity of infection. The epithelia used in these experiments were mainly composed of basal cells located at the base of the epithelium and ciliated columnar cells spanning the epithelium and providing the tight junctions. Analysis of vertical sections of several infectious centers consistently showed that in regions where all columnar cells were infected, no basal cells were infected (Figure 5B, arrows). Thus wild-type MV infects columnar cells that have formed tight junctions.

Wild-type MV is shed apically. In order to assess the polarity of viral release, the apical and basolateral surfaces of the WT_{green}-infected epithelial sheet were washed at regular time intervals. Viral titers were quantified by plaque formation on Vero/hSLAM cells. WT_{green} was released almost exclusively at the apical surface of the epithelium (Figure 6A), reaching approximately 10^4 PFU/ml between days 5 and 7 after inoculation, compared with approximately 50 PFU/ml released basolaterally. Infection did not compromise transepithelial resistance (Figure 6B), consistent with the lack of syncytia formation or other cytopathic effects. These data suggest that following basolateral infection, MV is preferentially shed apically into the airway lumen in vivo.

Discussion

We generated a shedding-incompetent MV. Toward this end, we identified and mutated amino acids of the MV attachment protein sustaining cell fusion through an unknown receptor, EpR. Hosts infected with the selectively EpR-blind virus developed rash and anorexia, while averaging slightly lower viremia than hosts infected with wild-type but did not shed virus in the airways. The EpR-blind virus did not enter well-differentiated human airway epithelial sheets basolaterally, the route of infection for wild-type MV.

Primary replication of all morbilliviruses can occur in SLAM-expressing lymphatic cells. The tonsils and buccal lymphatic tissue are the primary replication sites of CDV and RV (31, 32). A SLAM-blind CDV does not spread systemically and is completely attenuated (8). Recent macaque studies based on an MV expressing a fluorescent reporter protein documented early infection of lymphatic cells, confirming earlier studies in ferrets with a GFP-expressing CDV (10, 28).

Several H protein residues sustain EpR- but not SLAM-dependent fusion. They are located in an area distinct from that defined

Table 2
Clinical signs and detection of virus in secretions

Clinical signs	WT	WT-H_{DOUBLE}
Rash	Yes (2/6)	Yes (4/6)
Anorexia	Yes (3/6)	Yes (2/6)
Viremia	Yes (6/6)	Yes (6/6)
Virus in airways	Yes (6/6)[A]	No (0/6)

Data for rash, anorexia, and viremia of WT infections are from ref. 29; and for analysis of virus in the airways, from ref. 10. [A]See text.

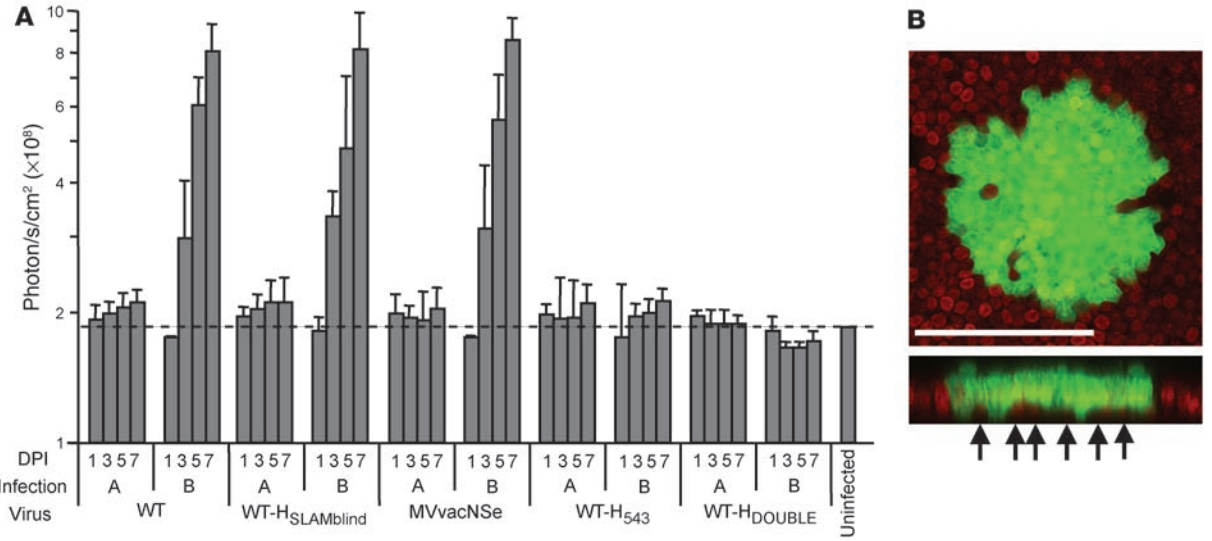

Figure 5

MV infects well-differentiated airway epithelium basolaterally and in an EpR-dependent fashion. (**A**) MV infection quantified by biofluorescence imaging following apical (A) or basolateral (B) infection. Measurements were performed on days 1, 3, 5, and 7 after infection (DPI) as indicated. Fluorescence intensity of GFP is expressed as the radiance units per second of photons leaving a square centimeter of tissue and radiating into a solid angle of 1 steradian (photons/s/cm²/sr). The dashed line indicates the average values of the uninfected sample. Error bars indicate mean ± SD. (**B**) Confocal imaging of basolaterally infected human primary airway epithelial cells. The cells were infected with the indicated viruses at an MOI of 0.1. The bottom panel is a vertical section of the top panel. Scale bar: 100 μm. Arrows indicate uninfected basal cells. Confocal images were captured with a Bio-Rad Radiance 2100 multiphoton confocal microscope.

by the SLAM-interacting amino acids. The H protein homodimer (25) has 2 tilted subunits exposing β-propeller blades 4, 5, and 6 upward toward the target cell (Figure 7, right; pink, light blue, and light green surfaces, respectively). The 3 EpR-relevant residues (red) define a small triangle located slightly above the equator. I194, the residue governing SLAM-binding (27), and the 4 residues involved in SLAM-dependent conformational changes (purple) (16) are located centrally on the top of each dimer. Most CD46-relevant residues (yellow) are in the bottom half. Thus the interaction of H with EpR involves blades 4 and 5, exposed upward toward the target cell.

We do not know which H residue is directly involved in EpR binding. Since 13%, 6%, and 17% of the surface of L482, P497, and Y543, respectively, are solvent exposed, we think that the minimally exposed proline 497 may conduct an EpR-dependent conformational change. Since the hydroxyl group on the aromatic ring of tyrosine 543 is solvent exposed, we generated an H protein with phenylalanine 543 and thus a hydrogen atom in place of the hydroxyl group. This protein completely lost EpR-specific fusion support while maintaining SLAM-dependent function (data not shown). Thus, the hydroxyl group on the aromatic ring of residue 543 may be involved in EpR binding.

Recently, Tahara et al. (12) identified F483, Y541, and Y543 as necessary for EpR-dependent fusion. We also found that mutation of Y541 or Y543 interferes with EpR-dependent fusion but noted that Y541 also reduces SLAM-dependent fusion. Together, our data and those of Tahara et al. (12) define a nonpolar valley running between propeller blades 4 and 5 (Figure 7, left panel). The nonpolar side chains of L482 (red), F483 (orange), and P497 (red), together with the uncharged polar side chains of Y541 (orange) and Y543 (red), flank this valley situated between the SLAM- and the CD46-binding sites. The hydroxyl group of tyrosine 543 tops one of the ridges and may directly support binding, while the other residues may do the same or contribute to subsequent receptor-specific conformational changes.

We showed that wild-type MV infected 2 lung and 1 bladder epithelium cell lines that were not polarized, eliciting cell fusion. Previous studies based on transformed cell lines reported that formation of a polarized monolayer interfered with apical infection (11, 12). We observed that after polarization of well-differentiated human airway epithelial sheets, MV infection occurs only basolaterally. Moreover, these epithelia did not form syncytia. Why? Two different mechanisms may slow down infection and restrict fusion efficiency. First, primary cells control infection better than transformed cells, limiting expression of viral proteins. Second, after cell polarization, EpR may move to a location less conductive to supporting fusion. We note that a precedent for cell-cell MV spread without visible fusion of the donor with the recipient cell exists (33).

We do not know the identity of EpR, but we know that in primary airway epithelial sheets, it is expressed only in ciliated columnar cells, which form tight junctions, but not in basal cells, which do not. At least 3 viral receptors are proteins with cell adhesion function located at tight junctions (34–37). If EpR is a basolateral protein sustaining epithelial function, the H-EpR interaction may result in destabilization of tight junctions, promoting massive release of immune cells in the airway lumen. The coughing host would aerosolize infected immune cells or viral particles, promoting contagion. This scenario implies limited viral replication in airway epithelia, and indeed necropsies of macaques performed 9 or 15 days after infection revealed restricted replication in epithelial cells, while infection of immune cells was massive (10). Thus, observations made in primary human airway epithelia and in primates are consistent with EpR being a basolateral protein in the columnar epithelial cells, which have formed tight junctions.

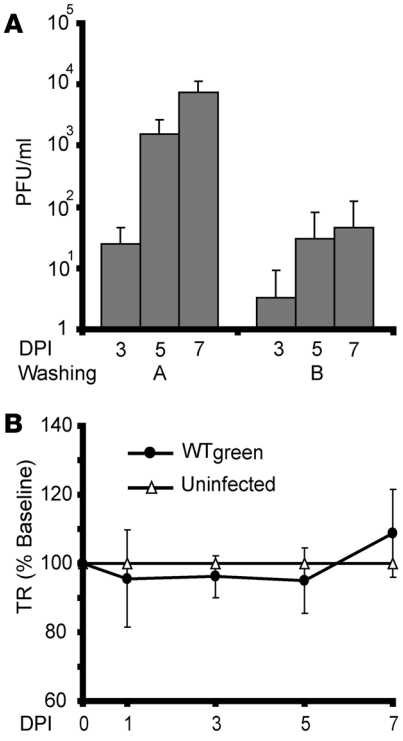

Figure 6
Polarity of virus release and human airway epithelium integrity. (**A**) Polarity of viral release following WT basolateral infection. Human airway epithelia were infected basolaterally, and both apical and basolateral washings were collected over the time intervals indicated. Washing titers were determined on Vero/hSLAM cells. Error bars represent SD. $n = 3$. (**B**) Maintenance of epithelial integrity following WT infection. The epithelial integrity was determined by volt-ohmmeter measurement of the transepithelial resistance (TR). Error bars represent SD. $n = 3$.

The shedding-incompetence principle established in our study may be applied to eliminate the potential of contagion from MV-based vectors used in cancer clinical trials. In current ovarian cancer, glioma, and myeloma clinical trials (38), patients cannot be in contact with unvaccinated infants or severely immunocompromised individuals until lack of shedding is established. Shedding-incompetent oncolytic viruses can be generated after transferring the EpR-inactivating mutations to a vaccine genetic background (39, 40). We note that the MV vaccine strain has 1-way epithelial crossing characteristics even if it binds CD46, which is abundantly expressed apically and basolaterally in epithelia (13). Thus, entry in polarized epithelial cells requires more than CD46 availability.

In conclusion, our results have confirmed the hypothesis of 1-way epithelial crossing by MV. Primary spread in immune cells followed by 1-way epithelia crossing may not be restricted to measles. Recent studies suggest that varicella-zoster virus may spread through T lymphocytes before replicating in epithelial cells (41). Vaccinia virus preferentially enters primary well-differentiated airway epithelia basolaterally, exits apically, and maintains epithelial integrity (42).

Methods

Cells. The human lung cell lines H358 (catalog no. CRL-5807; ATCC), H441 (HTB-174 ; ATCC), H23 (CRL-5800; ATCC), and H522 (CRL-5810; ATCC) were maintained in RPMI 1640 medium supplemented with 2 mM L-glutamine and adjusted to contain 1.5 g/l sodium bicarbonate, 4.5 g/l glucose, 10 mM HEPES, 1 mM sodium pyruvate, and 10% FCS. The human bladder cell line SCaBER (HTB-3; ATCC) was maintained in MEM supplemented with 2 mM L-glutamine and Earle's balanced salt solution (BSS) adjusted to contain 1.5 g/l sodium bicarbonate, 0.1 mM nonessential amino acids, 1 mM sodium pyruvate, and 10% FCS. The bladder cell line T24 (HTB-4;

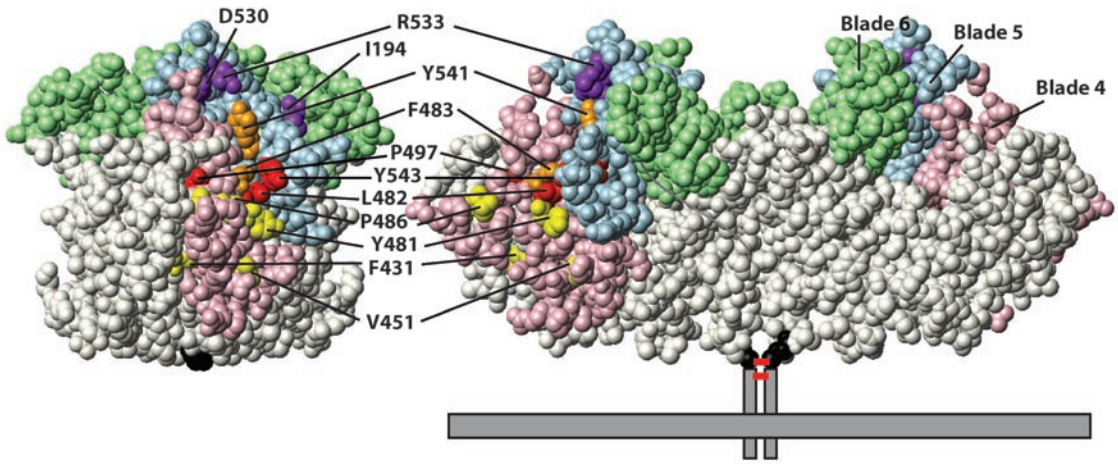

Figure 7
Space-filling representations of the solvent-accessible surface of MV Edmonston strain H protein structure with selectively receptor-sensitive amino acids. Right: side view of the homodimeric protein; left: left monomer after rotation of 90° in a mathematically positive direction around the *y* axis. The most relevant residues whose mutation selectively abolished receptor-dependent fusion are shown in red or orange (EpR), purple (SLAM), and yellow (CD46). The EpR-relevant residues identified by Tahara et al. (12) are shown in orange. The membrane is represented by a horizontal gray box; those parts of the H protein that were not crystallized (cytoplasmic tail, transmembrane domain, and part of the stalk; that is, amino acids 1–153) are shown by vertical gray boxes. The short red bars between the vertical boxes represent 2 disulfide bonds. The β-sheet propeller blades 4, 5, and 6 are in pink, light blue, and light green, respectively; the other blades are in white. Residue 154, anchor of the protein stalk region, is shown in black.

ATCC) was maintained in McCoy's 5A medium supplemented with 1.5 mM L-glutamine, 2.2 g/l sodium bicarbonate, and 10% FCS. The bladder cell line HT-1376 (CRL-1472; ATCC) was maintained in MEM with Earle's BSS, nonessential amino acids, and 10% FCS. Vero cells (African green monkey kidney; CCL-81; ATCC); HeLa cells (CCL-2; ATCC); and B95a, a marmoset B cell line kindly provided by D. Gerlier (University of Lyon 1, Lyon, France) were maintained in DMEM supplemented with 10% FCS. The rescue helper cell line 293-3-46 was grown in DMEM with 10% FCS and 1.2 mg of G418/ml. Vero/hSLAM cells, kindly provided by Y. Yanagi (Kyushu University, Fukuoka, Japan), were maintained in DMEM supplemented with 10% FCS and 0.5 mg of G418/ml.

Viruses. Recombinant viruses were recovered using the plasmid p(+)MV323, coding for the WT genome (43). Recombinant MVs were generated as previously described (44), but rescue cells were overlaid with cells expressing an appropriate receptor. Depending on the mutation, the viruses were propagated on Vero/hSLAM or H358 cells. To prepare virus stocks, Vero/hSLAM or H358 cells were infected at an MOI of 0.03 with the relevant virus and incubated at 37°C. Cells were scraped in Opti-MEM (Invitrogen) and particles released by 1 freeze-thaw cycle. Titers were determined by 50% end-point titration on Vero/hSLAM or H358 cells according to the Spearman-Kärber method (45).

Plasmids and mutagenesis. The expression plasmid pCG-IC323-H was obtained by digesting the plasmid p(+)MV323, coding for the WT genome, with the PacI/SpeI enzymes (Figure 1A). The DNA fragment encoding the *H* gene was subcloned into the PacI/SpeI-digested pCG plasmid (46). The plasmid pCG-IC323-F was produced by PCR amplification of the F ORF using the forward primer 5′-CCTTAATTAAATGGGTCTCAAGGTGAACGT-3′ (GenBank accession number NC_001498; underlined nucleotide at position 5,458) and reverse primer 5′-AGCTTTGTTTAAACTCAGAGCGACCTTACATAGGATT-3′ (underlined nucleotide at position 7,110), digesting the PCR product with PacI/PmeI enzymes, and subcloning the fragment into PacI/PmeI-digested pCG plasmid.

Mutations in the wild-type H ORF were introduced by QuikChange site-directed mutagenesis (Stratagene) using pCG-IC323-H as a template. For construction of the EGFP-expressing WT_{green}, a previously described additional transcription unit (19) was inserted in the EcoRV restriction site located at base 100 of the WT genome, upstream of the *N* gene. This additional transcription unit is composed of the complete EGFP ORF followed by the viral transcription stop sequence, the intergenic region, and the viral transcription start sequence identical to the sequence found between the *N* and *P* genes. Selected H mutants were transferred into the WT_{green} genome by moving the mutated PacI/SpeI fragment from pCG-IC323-H into PacI/SpeI-digested p(+)MV323 containing the additional transcription unit. All engineered MV genomes were of hexameric length.

Virus growth kinetics. Virus growth kinetics were determined at an MOI of 0.03 for 1 hour at 37°C. Infected cells were washed 3 times with Opti-MEM and returned to 37°C. At the indicated times, supernatants were clarified by centrifugation and cells scraped in Opti-MEM and subjected to 1 freeze-thaw cycle. Released and cell-associated viral titers were determined by $TCID_{50}$ titration.

Fusion assays. Cells seeded in 6-well tissue culture plates were allowed to reach 80% confluence prior to transfection. Equal amounts (2 μg) of pCG-IC323-F, the mutated pCG-IC323-H, and EGFP-expressing pEGFP-N1 (BD Biosciences — Clontech) were transfected using Lipofectamine 2000 (Invitrogen) according to the manufacturer's protocol. The extent of fusion was assessed by determining the proportion of cells in syncytia formation in representative fields of view 24 hours after transfection. The field-of-view area was 1,200 × 900 μm and typically contained 2,000 Vero/hSLAM cells or 1,300 H358 cells at the time of assessment. In Vero/hSLAM cells, a syncytium was defined as a cell with 5 or more nuclei. The levels of fusion in Vero/hSLAM are reported with the following notation (see Figure 2B): open rectangles, 2 or fewer syncytia per field of view; one-third-filled rectangle, less than 50% of the nuclei located in syncytia; two-thirds-filled rectangle, between 50% and 90% of the nuclei located in syncytia; completely filled rectangle, more than 90% of the nuclei located in syncytia. Since fusion was less extensive in H358 than in Vero/hSLAM cells, different thresholds were used, and only 2 levels of fusion above background were considered: open rectangles, no syncytia found; half-filled rectangle, less than 8% of the nuclei located in syncytia; completely filled rectangle, 9%–12% of the nuclei located in syncytia. A fusion score was assigned for each mutant after at least 3 independent experiments.

Homology modeling of the H protein. The procedure used to create the model of the MV Edmonston B vaccine lineage H protein based on the structure of the Newcastle disease virus hemagglutinin-neuraminidase (HN) protein (47) was published previously (16). The MV Edmonston B vaccine lineage H protein differs from the wild-type H protein by only 10 amino acids scattered over the whole sequence. The local side chain orientations close to these substitutions were expected to adjust without changing overall global folding. We therefore used the MV H–Newcastle disease virus HN protein alignment, replaced the sequence of the Edmonston B with the wild-type H protein, and generated a structural model as previously described (16). The model was further refined by energy minimization with FANTOM (48). The 3D representations of the structure were produced with MOLMOL software (49).

Infection of rhesus monkeys. Colony-bred male and female juvenile rhesus monkeys (*M. mulatta*), seronegative for MV, were housed in accordance with guidelines of the American Association for Accreditation of Laboratory Animal Care. All animal experiments were approved by the UC Davis Chancellor's Animal Use and Care Administrative Advisory Committee. For consistency with previous experiments, the $TCID_{50}$ of the virus stock was determined by endpoint dilution coculture with Raji cells, as described previously (50). Six animals were inoculated with $10^{4.5}$ $TCID_{50}$ of $WT\text{-}H_{DOUBLE}$ in a volume of 1 ml by a single drop onto the conjunctiva of each eye and the remainder divided into both nares. The animals were monitored daily for clinical symptoms including anorexia, depression, coughing, diarrhea, and skin rash. They were bled under ketamine sedation on days 0, 7, 14, 21, and 28 after inoculation, and viremia was quantified by end-point dilution coculture with Raji cells. Serial 10-fold dilutions of PBMCs were made in RPMI 1640 supplemented with 10% FCS and 1% glutamine, penicillin, and streptomycin (Sigma-Aldrich). Four replicates of 10^1 to 10^5 PBMCs were cocultured with 10^5 Raji cells per well in 24-well plates (Fisher Scientific), and 10^6 PBMCs were cocultured with 10^6 Raji cells in T25 flasks. The cultures were maintained for 2 weeks, monitored for large multinucleated giant cell formation, and scored for cytopathic effect by light microscopy (50). At the same time points, tracheal aspirates were taken and centrifuged and the cell pellet tested for MV by coculture with Raji cells. Neutralizing antibody against MV was measured as described previously (50).

Infection of polarized human airway epithelial cells. Primary cultures of human airway epithelia were prepared from trachea and bronchi by enzymatic dispersion and seeded onto collagen-coated, semipermeable membranes with an 0.4-μm pore size (Millicell-HA; surface area, 0.6 cm^2; Millipore Corp) as previously described (51). Only well-differentiated cultures (>2 weeks old; resistance, >500 cm^2) were used. Transepithelial resistance was measured with a volt-ohm meter (World Precision Instruments). Values were corrected for the blank filter resistance and further standardized against baseline readings and uninfected cultures. Neither corrected nor raw numbers resulted in a statistically significant variation from measurements in uninfected epithelia as determined by ANOVA.

MV preparations were diluted in sterile PBS to an MOI of 0.1, and 100 μl of the solution was applied to the apical or basolateral surface of airway epithelial cells (13). To provide similar opportunity of infection for both

sides of the cells, avoiding the negative effects of gravitation on particles added to the lower chamber, we inverted the filter prior to basolateral infection. After incubation for 4 hours at 37°C, the inoculum was removed, and cells were washed and further incubated at 37°C for the indicated time periods. A Xenogen IVIS CCD camera was used for biofluorescence imaging of infected cultures, and fluorescence intensity quantified using Xenogen Living Image software.

To determine the polarity of viral release from basolaterally infected epithelia, 500-μl washings were collected from both the apical and basolateral surfaces of epithelial sheets at progressive time points and used to infect Vero/hSLAM cells. Virus-inoculated plates were centrifuged at 200 *g* at room temperature for 10 minutes. Titers were calculated by counting EGFP-positive cells after 30 hours. Images of polarized epithelia were captured using a Bio-Rad Radiance 2100 confocal microscope.

Acknowledgments

We thank A. Arias, C. Wohlford-Lenane, C. Ondracek, and S. Vongpunsawad for assistance; Y. Yanagi for making the H protein structure available prior to publication; and V. von Messling for comments on the manuscript. This work was supported by NIH grants R01 CA090636 and R01 AI063476 (to R. Cattaneo), P51 RR11069 (to M.B. McChesney), K01 DK-073367 (to P.L. Sinn), R01 HL075363 (to P.B. McCray Jr.), and P01 HL-51670 (to P.B. McCray Jr.); and a grant from the Roy J. Carver Charitable Trust (to P.B. McCray Jr.). We also acknowledge the support of the Cell and Tissues and Cell Morphology Cores, partially supported by the Center for Gene Therapy for Cystic Fibrosis (NIH P30 DK-54759) and the Cystic Fibrosis Foundation.

Received for publication February 25, 2008, and accepted in revised form May 7, 2008.

Address correspondence to: Roberto Cattaneo, Mayo Clinic College of Medicine, Guggenheim 18, 200 First Street SW, Rochester, Minnesota 55905, USA. Phone: (507) 538-1188; Fax: (507) 266-2122; E-mail: cattaneo.roberto@mayo.edu.

1. Panum, P.L. 1939. Observations made during the epidemic of measles on the Faroe Islands in the year 1846. In *Medical classics.* Volume 3. E.C. Kelly, editor. Williams & Wilkins Co. Baltimore, Maryland, USA. **3**:803–886.
2. Cherry, J.D. 2004. Measles virus. In *Textbook of pediatric infectious diseases*. R.D. Feigin et al., editors. Elsevier Health Sciences. Philadelphia, Pennsylvania, USA. 2283–2304.
3. Griffin, D.E. 2007. Measles virus. In *Fields virology.* B.N. Fields, et al., editors. Lippincott Williams & Wilkins. Philadelphia, Pennsylvania, USA. 1551–1585.
4. Sherman, F.E., and Ruckle, G. 1958. In vivo and in vitro cellular changes specific for measles. *AMA Arch. Pathol.* **65**:587–599.
5. Sakaguchi, M., et al. 1986. Growth of measles virus in epithelial and lymphoid tissues of cynomolgus monkeys. *Microbiol. Immunol.* **30**:1067–1073.
6. McChesney, M.B., et al. 1997. Experimental measles. I. Pathogenesis in the normal and the immunized host. *Virology.* **233**:74–84.
7. Tatsuo, H., Ono, N., Tanaka, K., and Yanagi, Y. 2000. SLAM (CDw150) is a cellular receptor for measles virus. *Nature.* **406**:893–897.
8. von Messling, V., Svitek, N., and Cattaneo, R. 2006. Receptor (SLAM [CD150]) recognition and the V protein sustain swift lymphocyte-based invasion of mucosal tissue and lymphatic organs by a morbillivirus. *J. Virol.* **80**:6084–6092.
9. Yanagi, Y., Takeda, M., and Ohno, S. 2006. Measles virus: cellular receptors, tropism and pathogenesis. *J. Gen. Virol.* **87**:2767–2779.
10. de Swart, R.L., et al. 2007. Predominant infection of CD150+ lymphocytes and dendritic cells during measles virus infection of macaques. *PLoS Pathog.* **3**:e178.
11. Maisner, A., Klenk, H., and Herrler, G. 1998. Polarized budding of measles virus is not determined by viral surface glycoproteins. *J. Virol.* **72**:5276–5278.
12. Tahara, M., et al. 2008. Measles virus infects both polarized epithelial and immune cells using distinctive receptor-binding sites on its hemagglutinin. *J. Virol.* **82**:4630–4637.
13. Sinn, P.L., Williams, G., Vongpunsawad, S., Cattaneo, R., and McCray, P.B., Jr. 2002. Measles virus preferentially transduces the basolateral surface of well-differentiated human airway epithelia. *J. Virol.* **76**:2403–2409.
14. Cattaneo, R., and Rose, J.K. 1993. Cell fusion by the envelope glycoproteins of persistent measles viruses which caused lethal human brain disease. *J. Virol.* **67**:1493–1502.
15. Wild, T.F., Malvoisin, E., and Buckland, R. 1991. Measles virus: both the haemagglutinin and fusion glycoproteins are required for fusion. *J. Gen. Virol.* **72**:439–442.
16. Vongpunsawad, S., Oezgun, N., Braun, W., and Cattaneo, R. 2004. Selectively receptor-blind measles viruses: identification of residues necessary for SLAM- or CD46-induced fusion and their localization on a new hemagglutinin structural model. *J. Virol.* **78**:302–313.
17. Naniche, D., et al. 1993. Human membrane cofactor protein (CD46) acts as a cellular receptor for measles virus. *J. Virol.* **67**:6025–6032.
18. Dorig, R.E., Marcil, A., Chopra, A., and Richardson, C.D. 1993. The human CD46 molecule is a receptor for measles virus (Edmonston strain). *Cell.* **75**:295–305.
19. Duprex, W.P., McQuaid, S., Hangartner, L., Billeter, M.A., and Rima, B.K. 1999. Observation of measles virus cell-to-cell spread in astrocytoma cells by using a green fluorescent protein-expressing recombinant virus. *J. Virol.* **73**:9568–9575.
20. Condack, C., Grivel, J.C., Devaux, P., Margolis, L., and Cattaneo, R. 2007. Measles virus vaccine attenuation: suboptimal infection of lymphatic tissue and tropism alteration. *J. Infect. Dis.* **196**:541–549.
21. Takeda, M., et al. 2007. A human lung carcinoma cell line supports efficient measles virus growth and syncytium formation via SLAM- and CD46-independent mechanism. *J. Virol.* **81**:12091–12096.
22. Sheshberadaran, H., and Norrby, E. 1986. Characterization of epitopes on the measles virus hemagglutinin. *Virology.* **152**:58–65.
23. Hu, A., Sheshberadaran, H., Norrby, E., and Kovamees, J. 1993. Molecular characterization of epitopes on the measles virus hemagglutinin protein. *Virology.* **192**:351–354.
24. Santiago, C., Bjorling, E., Stehle, T., and Casasnovas, J.M. 2002. Distinct kinetics for binding of the CD46 and SLAM receptors to overlapping sites in the measles virus hemagglutinin protein. *J. Biol. Chem.* **277**:32294–32301.
25. Hashiguchi, T., et al. 2007. Crystal structure of measles virus hemagglutinin provides insight into effective vaccines. *Proc. Natl. Acad. Sci. U. S. A.* **104**:19535–19540.
26. Colf, L.A., Juo, Z.S., and Garcia, K.C. 2007. Structure of the measles virus hemagglutinin. *Nat. Struct. Mol. Biol.* **14**:1227–1228.
27. Navaratnarajah, C.K., et al. 2008. Dynamic interaction of the measles virus hemagglutinin with its receptor signaling lymphocytic activation molecule (SLAM, CD150). *J. Biol. Chem.* **283**:11763–11771.
28. von Messling, V., Milosevic, D., and Cattaneo, R. 2004. Tropism illuminated: lymphocyte-based pathways blazed by lethal morbillivirus through the host immune system. *Proc. Natl. Acad. Sci. U. S. A.* **101**:14216–14221.
29. Devaux, P., Hodge, G., McChesney, M.B., and Cattaneo, R. 2008. Attenuation of v- or C-defective measles viruses: infection control by the inflammatory and interferon responses of rhesus monkeys. *J. Virol.* **82**:5359–5367.
30. Karp, P.H., et al. 2002. An in vitro model of differentiated human airway epithelia. Methods for establishing primary cultures. *Methods Mol. Biol.* **188**:115–137.
31. Plowright, W. 1964. Studies on the pathogenesis of rinderpest in experimental cattle. II. Proliferation of the virus in different tissues following intranasal infection. *J. Hyg. (Lond.)* **62**:257–281.
32. Appel, M.J. 1969. Pathogenesis of canine distemper. *Am. J. Vet. Res.* **30**:1167–1182.
33. Firsching, R., et al. 1999. Measles virus spread by cell-cell contacts: uncoupling of contact-mediated receptor (CD46) downregulation from virus uptake. *J. Virol.* **73**:5265–5273.
34. Barton, E.S., et al. 2001. Junction adhesion molecule is a receptor for reovirus. *Cell.* **104**:441–451.
35. Coyne, C.B., and Bergelson, J.M. 2006. Virus-induced Abl and Fyn kinase signals permit coxsackievirus entry through epithelial tight junctions. *Cell.* **124**:119–131.
36. Walters, R.W., et al. 2002. Adenovirus fiber disrupts CAR-mediated intercellular adhesion allowing virus escape. *Cell.* **110**:789–799.
37. Evans, M.J., et al. 2007. Claudin-1 is a hepatitis C virus co-receptor required for a late step in entry. *Nature.* **446**:801–805.
38. Liu, T.C., Galanis, E., and Kirn, D. 2007. Clinical trial results with oncolytic virotherapy: a century of promise, a decade of progress. *Nat. Clin. Pract. Oncol.* **4**:101–117.
39. Devaux, P., von Messling, V., Songsungthong, W., Springfeld, C., and Cattaneo, R. 2007. Tyrosine 110 in the measles virus phosphoprotein is required to block STAT1 phosphorylation. *Virology.* **360**:72–83.
40. Reyes del Valle, J., et al. 2007. A vectored measles virus induces hepatitis B surface antigen antibodies while protecting macaques against measles virus challenge. *J. Virol.* **81**:10597–10605.
41. Cohen, J.I., Straus, S.E., and Arvin, A.M. 2007. Varicella-zoster virus. In *Fields virology.* B.N. Fields, et al., editors. Lippincott Williams & Wilkins. Philadelphia, Pennsylvania, USA. 2773–2818.
42. Vermeer, P.D., et al. 2007. Vaccinia virus entry, exit, and interaction with differentiated human airway epithelia. *J. Virol.* **81**:9891–9899.
43. Takeda, M., et al. 2000. Recovery of pathogenic measles virus from cloned cDNA. *J. Virol.* **74**:6643–6647.

44. Radecke, F., et al. 1995. Rescue of measles viruses from cloned DNA. *EMBO J.* **14**:5773–5784.
45. Kärber, G. 1931. Beitrag zur kollektiven Behandlung pharmakologischer Reihenversuche. *Arch. Exp. Pathol. Pharmakol.* **162**:480–483.
46. Huber, M., et al. 1991. Measles virus phosphoprotein retains the nucleocapsid protein in the cytoplasm. *Virology.* **185**:299–308.
47. Crennell, S., Takimoto, T., Portner, A., and Taylor, G. 2000. Crystal structure of the multifunctional paramyxovirus hemagglutinin-neuraminidase. *Nat. Struct. Biol.* **7**:1068–1074.
48. Thomas, S., Braun, W., and Wüthrich, K. 1990. The program FANTOM for energy refinement of polypeptides and proteins using a Newton-Raphson minimizer in torsion angle space. *Biopolymers.* **29**:679–694.
49. Koradi, R., Billeter, M., and Wuthrich, K. 1996. MOLMOL: a program for display and analysis of macromolecular structures. *J. Mol. Graph.* **14**:51–55.
50. Zhu, Y.D., et al. 1997. Experimental measles. II. Infection and immunity in the rhesus macaque. *Virology.* **233**:85–92.
51. Zabner, J., Zeiher, B.G., Friedman, E., and Welsh, M.J. 1996. Adenovirus-mediated gene transfer to ciliated airway epithelia requires prolonged incubation time. *J. Virol.* **70**:6994–7003.